

Use of dansyl-cholestanol as a probe of cholesterol behavior in membranes of living cells^S

Huan Huang,* Avery L. McIntosh,* Barbara P. Atshaves,[§] Yoshiko Ohno-Iwashita,** Ann B. Kier,[†] and Friedhelm Schroeder^{1,*}

Department of Physiology and Pharmacology,* and Department of Pathobiology,[†] Texas A&M University, TVMC, College Station, TX 77843; Department of Biochemistry and Molecular Biology,[§] Michigan State University, East Lansing, MI 48824; and Biomembrane Research Group,** Tokyo Metropolitan Institute of Gerontology, Tokyo 173-0015, Japan

Abstract While plasma membrane cholesterol-rich microdomains play a role in cholesterol trafficking, little is known about the appearance and dynamics of cholesterol through these domains in living cells. The fluorescent cholesterol analog 6-dansyl-cholestanol (DChol), its biochemical fractionation, and confocal imaging of L-cell fibroblasts contributed the following new insights: i) fluorescence properties of DChol were sensitive to microenvironment polarity and mobility; ii) DChol taken up by L-cell fibroblasts was distributed similarly as cholesterol and preferentially into cholesterol-rich vs. -poor microdomains resolved by affinity chromatography of purified plasma membranes; iii) DChol reported similar polarity (dielectric constant near 18) but higher mobility near phospholipid polar head group region for cholesterol in purified cholesterol-rich versus -poor microdomains; and iv) real-time confocal imaging, quantitative colocalization analysis, and fluorescence resonance energy transfer with cholesterol-rich and -poor microdomain markers confirmed that DChol preferentially localized in plasma membrane cholesterol-rich microdomains of living cells. **¶¶** Thus, DChol sensed a unique, relatively more mobile microenvironment for cholesterol in plasma membrane cholesterol-rich microdomains, consistent with the known, more rapid exchange dynamics of cholesterol from cholesterol-rich than -poor microdomains.—Huang, H., A. L. McIntosh, B. P. Atshaves, Y. Ohno-Iwashita, A. B. Kier, and F. Schroeder. Use of dansyl-cholestanol as a probe of cholesterol behavior in membranes of living cells. *J. Lipid Res.* 2010. 51: 1157–1172.

Supplementary key words plasma membrane • fluorescence • imaging • fibroblasts • FRET • affinity chromatography

While the original bilayer theory of lipid membrane structure envisioned proteins imbedded in a sea of randomly organized lipids, subsequent reports increasingly

This work was supported in part by the USPHS National Institutes of Health GM-31651 (to F.S. and A.B.K.) and DK-70965 (to B.P.A.). Its contents are solely the responsibility of the authors and do not necessarily represent the official views of the National Institutes of Health or other granting agencies.

Manuscript received 16 October 2009 and in revised form 11 December 2009.

*Published, JLR Papers in Press, December 11, 2009
DOI 10.1194/jlr.M003244*

demonstrated that membrane lipids are asymmetrically organized both across the bilayer and laterally within the bilayer into discrete microdomains (1–4). Recent model membrane studies indicate that both cholesterol and sphingolipids undergo lateral phase separation to form microdomains rich and poor in these respective lipids (5, 6). Purified plasma membrane cholesterol-rich microdomains are enriched in proteins facilitating the transport of cholesterol (7–10), fatty acids (11), and glucose (12, 13). Key plasma membrane proteins that facilitate reverse cholesterol transport [e.g., caveolin-1, scavenger receptor B1 (SRB1), ATP-binding cassette transport protein A1 (ABCA1), and P-glycoprotein (P-gp)] are localized in cholesterol-rich microdomains isolated from cells or purified plasma membranes (6, 7, 10). Disruption of cholesterol-rich microdomains inhibits SRB1-mediated cholesterol transport (6, 7, 10).

Despite these advances with biochemically isolated cholesterol-rich and -poor microdomains, the lack of readily measurable parameters for cholesterol makes direct real-time imaging of cholesterol and cholesterol-dynamics through these microdomains in living cells very difficult (14–16). Although the behavior of cholesterol has been examined by a variety of techniques in model membranes, many are not useful for living systems, because they require extreme conditions (vacuum), probes with mobility

Abbreviations: BC_θ, biotinylated C_θ-toxin; con-A, Concanavalin-A; Ct-B, cholera toxin subunit B; DChol, 6-dansyl-cholestanol; DHE, dehydroergosterol; DiI_{1,1'}, 1,1'-dioctadecyl-3,3,3',3'-tetramethylindodicarbocyanine, 4-chlorobenzenesulfonate salt (DiI_{C₁₈(5)}); FRET, fluorescence resonance energy transfer; LSCM, laser scanning confocal microscopy; LUV, large unilamellar vesicle; M_βCD, methyl- β -cyclodextrin; NBD-cholesterol, 22-(N-(7-nitrobenz-2-oxa-1,3-diazol-4-yl)amino)-23,24-bisnor-5-cholen-3 β -ol; Pgp, P-glycoprotein; POPC, 1-palmitoyl-2-oleoyl-phosphatidylcholine; N-Rh-DOPE, 1,2-dioleoyl-sn-glycero-3-phosphoethanolamine-N-(lissamine rhodamine B sulfonyl) (ammonium salt); SRB1, scavenger receptor B1.

¹To whom correspondence should be addressed.

e-mail: fschroeder@cvm.tamu.edu

S The online version of this article (available at <http://www.jlr.org>) contains supplementary data in the form of six supplementary methods and two figures.

that involves time scales too slow for determining cholesterol dynamics in living systems, and use of sterol analogs that may not mimic the behavior of cholesterol (17, 18). While the naturally occurring fluorescent dehydroergosterol (DHE) mimics the behavior of cholesterol, especially in codistributing with cholesterol in purified cholesterol-rich and -poor microdomains isolated from plasma membranes, DHE unfortunately has low quantum yield, is easily bleached, absorbs in the UV (i.e., near 325 nm), requires multiphoton excitation for imaging in living cells, and is not sensitive to the polarity of its environment (6, 14–16). Other fluorescent sterols such as 22-(N-(7-nitrobenz-2-oxa-1,3-diazol-4-yl)amino)-23,24-bisnor-5-cholesterol (NBD)-cholesterol distribute poorly into membranes and preferentially localize in lipid droplets within the cytoplasm (14–16).

To begin to address these issues, the current study took advantage of the unique fluorescence properties of 6-dansyl-cholesterol (DChol) to determine the structure and polarity sensed by cholesterol in cholesterol-rich and -poor microdomains and to use real-time confocal imaging to explore cholesterol dynamics and trafficking through cholesterol-rich versus -poor microdomains in the plasma membrane of living cells. The results showed that: i) fluorescence properties of DChol were sensitive to microenvironment polarity and mobility; ii) DChol was taken up by L-cell fibroblasts and distributed preferentially and similarly as cholesterol into cholesterol-rich versus -poor microdomains resolved from purified plasma membranes by affinity chromatography; iii) DChol reported similar polarity but higher mobility near the phospholipid polar head group region, for cholesterol in purified cholesterol-rich versus -poor microdomains; and iv) real-time confocal imaging, quantitative colocalization analysis, and fluorescence resonance energy transfer (FRET) with cholesterol-rich and -poor microdomain markers confirmed that DChol preferentially localized in plasma membrane cholesterol-rich microdomains of living cells.

METHODS

Materials

1-Palmitoyl-2-oleoyl-phosphatidylcholine (POPC) and 1,2-dioleoyl-sn-glycero-3-phosphoethanolamine-N-(lissamine rhodamine B sulfonyl) (ammonium salt) (Rh-DOPE) were purchased from Avanti Polar Lipids (Alabaster, AL). Methyl- β -cyclodextrin (M β CD), cholesterol, and 6-ketocholesterol were acquired from Sigma (St. Louis, MO). Vybrant DiD labeling solution, Vybrant Alexa Fluor 594 CT-B Kit, and Alexa Fluor 660 streptavidin were obtained from Invitrogen Corporation (Carlsbad, CA). Biotinylated C θ -toxin (BC θ), a biotinylated perfringolysin O derivative, was prepared by Dr. Yoshiko Ohno-Iwashita (Tokyo Metropolitan Institute of Gerontology, Japan) as described earlier (19). DHE was synthesized by a modification of an established procedure as described earlier (15). Concanavalin-A (con-A) sepharose 4B resin and Percoll were purchased from GE Healthcare Bio-Sciences Corp. (Piscataway, NJ); silica gel G TLC plates were from Analtech (Newark, DE). All reagents and solvents used were of the highest grade available and were cell culture tested.

DChol synthesis

DChol is a structural analog of cholesterol with the dansyl group attached at position 6 of cholesterol (Fig. 1A). DChol was synthesized and purified based on a previously published method (20) with some modifications (for details, see supplementary Method I).

Determination of critical micelle concentration of cholesterol and DChol

The critical micelle concentration of cholesterol and DChol were determined by measuring light scatter as a function of increasing cholesterol or DChol concentrations in water. The details of the critical micelle concentration measurements can be found in supplementary Method II.

Incorporation of DChol into cultured L-cells

Murine L-cells (L arptk) were cultured with Hguchi medium containing 10% fetal bovine serum (Invitrogen) and grown to confluence at 37°C with 5% CO₂ in a humidified incubator as described earlier (21). For real-time imaging, cells were seeded onto Lab-Tek two-chambered cover-glass (Nunc, Naperville, IL or VWR Scientific, Sugarland, TX) at a density of 25,000–50,000 cells/chamber and were cultured for 36–48 h (22). Like cholesterol, DChol has poor solubility in aqueous media; therefore, DChol was complexed with M β CD to facilitate uptake by cultured L-cells. DChol-M β CD complex was prepared according to a published procedure (20). Because M β CD alone can extract cholesterol from membranes (23), the DChol-M β CD complexes used herein were prepared at molar ratios of DChol-M β CD that did not result in net change in total cell sterol (24). To incorporate DChol into cultured L-cells for imaging, cells were incubated with DChol-M β CD complex (DChol concentration 4–20 μ g/ml) at room temperature in PBS for 15 min unless otherwise specified.

Determination of apparent binding constants of cholesterol and DChol to M β CD

For details, see supplementary Method III.

Esterification of DChol by cultured L-cells

To determine if L-cells esterify DChol, L-cells were incubated with DChol-M β CD (DChol final concentration 20 μ g/ml) for the amount of time as specified. Lipids were extracted according to previously published procedures (22). The unesterified sterol (DChol, Chol) was separated from esterified sterol (DChol esters, Chol-esters) using TLC silica gel G plates. Known amounts of unesterified and esterified sterol standards (Chol, Chol-ester, and DChol) were spotted on separate lanes on the same TLC plate to construct the standard curves for quantification. The TLC plate was developed in heptane-diethyl ether-methanol-acetic acid (80:35:3:2) (20). Fluorescent spots were visualized and quantitated with FluoChem imaging system and software. To identify fatty acids esterified to the sterols, spots corresponding to Chol-esters and DChol-esters were scraped, transesterified, and analyzed by GC/MS using a Trace DSQ single quadrupole GC/MS with electron impact and chemical ionization sources (Thermo Electron, Austin, TX) in chemical ionization mode basically as described earlier (25).

Affinity chromatography of purified plasma membranes to resolve cholesterol-rich and -poor microdomains

DChol was incorporated into L-cells as described above. Plasma membranes were then isolated followed by nondetergent, affinity-chromatography to resolve cholesterol-rich and -poor microdomain-enriched fractions using con-A sepharose columns

according to previously established procedures (22, 26–28). Lipids in each fraction were then extracted as described above followed by resolution by TLC and quantitation of DChol and cholesterol as described above and in earlier publications (22, 29).

DChol fluorescence excitation, emission, polarization, and light scatter

Fluorescence excitation spectra, emission spectra, polarization and anisotropy, and light scatter measurements were obtained with an ISS PCI photon counting fluorimeter (ISS Instruments Inc., Champaign, IL) basically as described earlier for DHE and other fluorescent probes (30–34). All measurements were recorded at 24°C with the exception of light scatter, which was determined at 37°C with a circulating water bath. DChol excitation and emission maxima were 340 nm and 520 nm, respectively. Light scatter was measured by setting both excitation and emission wavelengths at 380 nm. All measurements were made below 0.15 absorbance units (to avoid inner filter effects) and corrected for the appropriate blanks.

L-cell labeling with different membrane domain markers

To study DChol colocalization and FRET with different membrane domain markers, L-cells were labeled with DChol only (as described above), membrane marker only, and both, respectively. The following markers were chosen for this study: Alexa Fluor cholera toxin subunit B (CT-B; a cholesterol-rich microdomain marker that binds to GM1); 1,1'-dioctadecyl-3,3',3'-tetramethylindodicarbocyanine, 4-chlorobenzenesulfonate salt (DiI₁₈(5)) (DiD; a liquid ordered phase marker); DHE (naturally occurring fluorescent cholesterol analog that codistributes with cholesterol in lipid cholesterol-rich and -poor microdomains); BC0 (specifically binds to cholesterol in cholesterol-rich domains); and N-Rh-DOPE (a marker for fluid or liquid disordered phase in lipid bilayers). L-cell labeling with Alexa Fluor 594 CT-B and DiD was done according to the manufacturer's instructions (Molecular Probes, Eugene, OR). L-cell labeling with DHE was done by incubation with DHE-MβCD (DHE concentration 20 μg/ml) in PBS at room temperature for 45 min. L-cell labeling with Alexa Fluor 660 BC0 was done as previously described (19). L-cell labeling with N-Rh-DOPE was done by incubation at 2°C (0.8 μM) for 15 min by ethanol injection method as described in an earlier publication (35).

Laser scanning confocal microscopy and multiphoton laser scanning microscopy

Images of DChol and most other probes were obtained by laser scanning confocal microscopy (LSCM) using an Axiovert 135 microscope (Zeiss; Carl Zeiss Inc., Thornwood, NY) and MRC-1024MP LSCM fluorescence imaging system (Bio-Rad, Hercules, CA) equipped with an external detection system (29, 36). The laser lines used for excitation were: 408 nm for DChol, 568 nm for Alexa Fluor 594 CT-B and N-Rh-DOPE, and 648 nm for Alexa Fluor 660 BC0 and DiD. The emission filters were: HQ530/40 for DChol, HQ598/40 for Alexa 594 CT-B and N-Rh-DOPE, and 680/32 for Alexa Fluor 660 BC0 and DiD. DHE was imaged by multiphoton laser scanning microscopy as described previously using a Coherent Mira 900F Ti:sapphire laser pumped at 10 W with a Spectra-Physics Millennia Classic laser (Newport, Santa Clara, CA) (37, 38). All images were acquired in PBS at room temperature and analyzed using LaserSharp (Bio-Rad Inc., Hercules, CA) and MetaMorph Image Analysis (Advanced Scientific Imaging, Merieux, LA) software. Fluorescent intensity in images of single living cells was expressed as the mean fluorescence intensity in gray scale units ± SE. Colocalization was determined by

superposition of images of DChol and the fluorescent membrane probe obtained through two different channels similarly as described for other fluorescent lipid probes (29, 36). Quantitative analysis of DChol fluorescence in cholesterol-rich and -poor microdomains and quantitative colocalization analysis can be found in supplementary Method IV.

FRET between DChol and DHE in large unilamellar vesicles

Significant overlap between DHE emission spectrum and DChol excitation spectrum allowed the use of FRET to determine if DChol codistributed in proximity to DHE. In this FRET study, DHE was chosen as donor and DChol as acceptor. Large unilamellar vesicle (LUVs) were prepared with 65% POPC, 5% DHE, 0.1–10% DChol, and cholesterol to make the total sterol content to be 35%. Corresponding LUVs made with i) no fluorescence sterols, ii) 5% DHE, and iii) 0.1–10% DChol were used as controls. Fluorescence measurements were conducted with PCI fluorimeter, excitation was set at 300 nm, and emission was measured at 325–575 nm at 37°C with a circulating water bath. The emission spectrum of control LUVs (0.1–10% DChol only) were subtracted from emission spectrum of sample LUVs to correct for emission from direct DChol excitation. Energy transfer efficiency $E\%$ were calculated by $E = 1 - I_{DA}/I_D$, where I_{DA} is donor DHE fluorescence intensity at 373 nm in the presence of acceptor DChol and I_D is DHE fluorescence intensity at 373 nm in the absence of DChol.

Next, the experimental results were compared with the data calculated for a random distribution of DChol relative to DHE in the LUV bilayer. The efficiency of energy transfer is determined mathematically (details can be found in supplementary Method V). MathCAD 14 (PTC Corporation, Needham, MA) was used for numerical calculations to determine efficiency of energy transfer based upon the calculated $R_0 = R_{2/3}$, R_{min} , and R_{max} and the values were subsequently graphed as a function of DChol% (mol%).

DChol FRET with different membrane probes in living cells

The chosen membrane domain probes all have significant spectral overlap with DChol to permit fluorescence energy transfer. Fluorescence energy transfer was determined for the following pairs: DChol as donor, Alexa Fluor CT-B, DiD, Alexa Fluor 660 BC0, and N-Rh-DOPE as acceptors, respectively; DHE as donor, and DChol as acceptor. Cells labeled with both the donor and the acceptor were excited at donor excitation wavelength, and FRET was observed as increase in acceptor emission and/or decrease in donor emission. For the probes relatively easy to photobleach (such as N-Rh-DOPE), acceptor photobleaching was also used to see if there was increase in donor emission upon acceptor photobleaching. Controls were run with donor only and acceptor only samples to ensure spectral bleed through was eliminated or corrected.

Real-time fluorescence imaging of DChol uptake through plasma membrane cholesterol-rich and -poor microdomains of living L-cell fibroblasts

To determine if DChol/MβCD complexes mediated DChol uptake into L-cells primarily through cholesterol-rich or -poor microdomains, L-cells were first labeled with Alexa Fluor CT-B as described above, then were incubated with DChol-MβCD (DChol concentration 10 μg/ml) in PBS. After DChol addition, images were acquired continuously for the first 15 min at room temperature. Images of Alexa Fluor 594 CT-B (Ex 568 nm, Em HQ598/40 filter) were acquired simultaneously with DChol (Ex 408 nm, Em HQ530/40 filter) through separate photomultipliers. DChol in cholesterol-rich and -poor microdomains was obtained by mea-

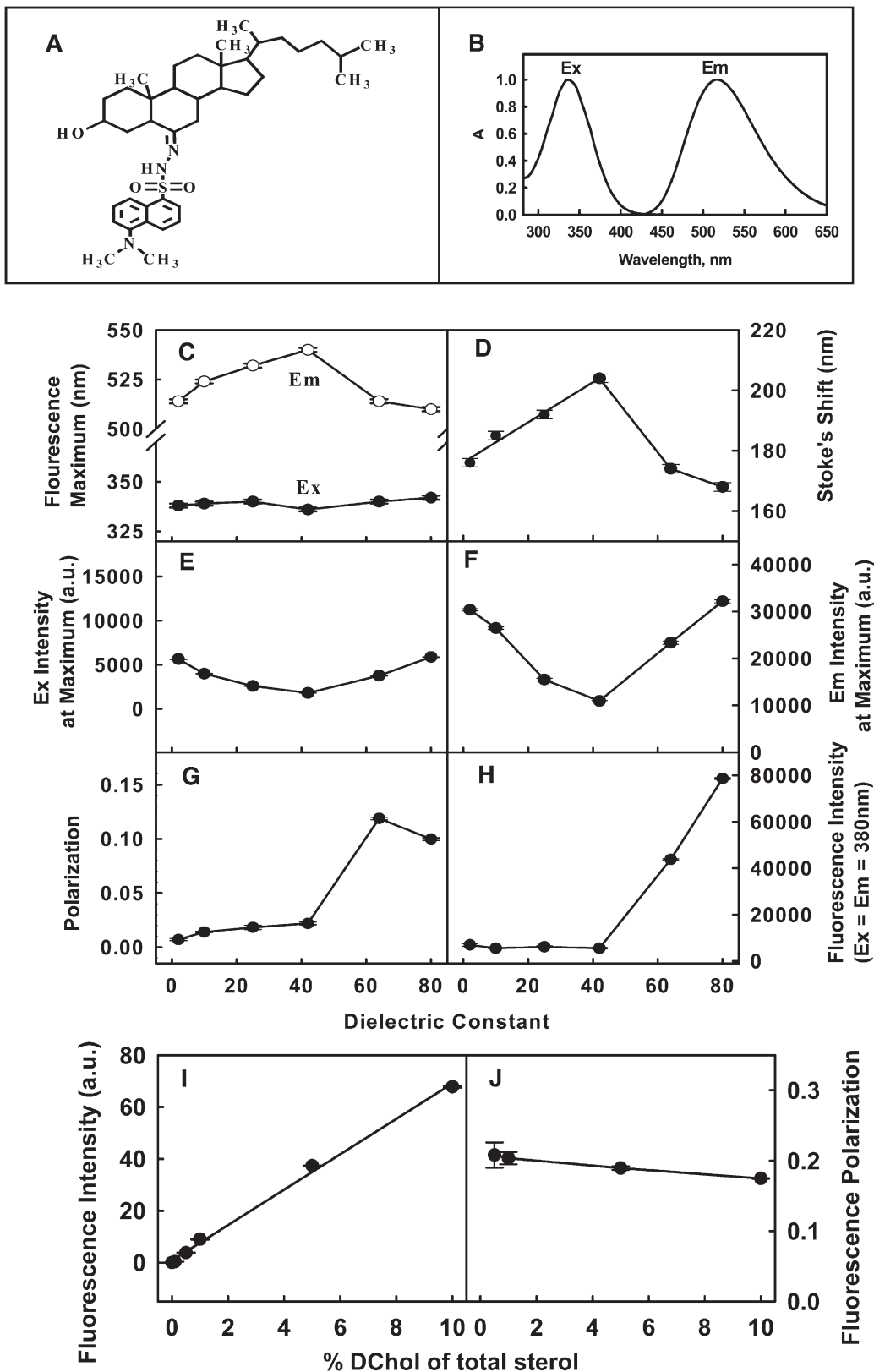


Fig. 1. Structure and fluorescence properties of DChol. **A:** Structure of DChol. The properties of DChol in solvents are shown in **B–H** as follows. **B:** Excitation and emission spectra of DChol in ethanol (5 $\mu\text{g}/\text{ml}$). Effect of solvent polarity (100% to 0% dioxane in water) on DChol (5 $\mu\text{g}/\text{ml}$) excitation and emission maximum (**C**), Stokes shift (**D**), fluorescence excitation intensity at maximum (**E**), fluorescence emission intensity at maximum (**F**), polarization changes (**G**), and light scattering (**H**). The properties of DChol in LUV are shown in **I** and **J**. LUV (POPC:total sterol = 65:35) were prepared with increasing DChol (0.1–10% of total sterol). **I:** Maximal fluorescence emission intensity (excitation at 336 nm) of DChol in LUV with increasing amount of DChol. **J:** Fluorescence polarization of DChol (excitation at 336 nm; emission at 522 nm) of DChol in LUV with increasing of DChol.

suring fluorescence intensity of pixels in the plasma membrane that were colocalized and not colocalized with cholesterol-rich microdomain marker Alexa Fluor 594 CT-B, respectively, as described above. Average DChol fluorescence intensities in whole cell, plasma membrane, intracellular region, and-cholesterol-rich and -poor microdomains versus time were plotted.

RESULTS

DChol in aqueous buffers

Fluorescence excitation and emission maxima of the purified DChol in ethanol were 336 nm and 522 nm, respectively (Fig. 1B). Fluorescence spectral properties of dansyl groups attached to proteins and polar lipids are strongly dependent on solvent polarity and order (39, 40). To study if DChol behaves similarly, spectra of DChol were recorded in dioxane-water mixtures wherein the dielectric constant ranged from 2 (100% dioxane) to 80 (100% water). As shown in Fig. 1C, whereas DChol fluorescence excitation maximum changed very little, its emission maximum was highly responsive to solvent polarity. As the solvent dielectric constant increased from 2 to 42, the emission maximum of DChol was red shifted by 26 nm. However, further increasing solvent polarity to dielectric constant 80 blue shifted the DChol emission maximum by 4 nm. The latter was most likely due to the limited aqueous solubility of the DChol resulting in formation of micelles/microcrystals as solvent polarity exceeded that of dielectric constant 40. This was confirmed by light scatter and polarization measurements (as will be discussed below). When DChol was not micellar (i.e., dielectric constant 2–40), DChol Stokes shifts (i.e., difference between excitation and emission wavelength at maximum) increased linearly with the dielectric constant (Fig. 1D).

In addition to DChol emission wavelength sensitivity, the maximal fluorescence excitation and emission intensities of DChol were also responsive to solvent polarity (Fig. 1E, F). When solvent dielectric constant increased from 2 to 42, the DChol maximal excitation intensity (Fig. 1E) and maximal emission intensity (Fig. 1F) were decreased nearly 70%. However, as the polarity of the solvent was further increased, the DChol excitation and emission maximum intensity increased (Fig. 1E, F), again consistent with micellization of DChol at solvent polarity greater than dielectric constant of 40.

Fluorescence polarization (i.e., anisotropy) and light scatter measurements confirmed the formation of DChol micelles/microcrystals at solvent dielectric constant ≥ 40 . DChol polarization in the most nonpolar environment was very low (near 0.007 in solvent of dielectric constant 2), consistent with mobility of DChol monomers in isotropic solvent (Fig. 1G), and increased very slowly as the solvent dielectric constant increased to 40. When solvent dielectric constant further increased ≥ 40 , DChol polarization increased much more dramatically, consistent with a more ordered/rigid microenvironment. Increased light scattering at dielectric constant ≥ 40 (Fig. 1H) also indicated formation of larger particles or aggregation. Therefore, polarization and light scattering data both are

consistent with formation of DChol micelles/microcrystals at solvent dielectric constant ≥ 40 .

To further establish that the tendency of DChol to form micelles/microcrystals in polar solvents was similar to other fluorescent sterols and to cholesterol, light scatter measurements were performed to determine the critical concentration at which DChol form micelles/microcrystals. The results showed that this critical concentration was near 155 nM for DChol and 35 nM for cholesterol (supplementary Fig. 1). The result for cholesterol was consistent with previously published data (41). Thus, similar to other fluorescent sterols (15, 16, 42), DChol exhibited a somewhat higher critical concentration for micelle/microcrystal formation in aqueous buffer than exhibited by cholesterol. Nevertheless, DChol, like cholesterol and other fluorescent sterols, was very poorly soluble in aqueous buffer.

The above results indicated that the spectral properties of the dansyl group present in DChol were greatly affected by polarity and structure of the environment: i) DChol exhibit the smallest Stokes' shift and highest fluorescence intensity in most hydrophobic environments (100% dioxane or micelle); ii) DChol showed the largest Stokes' shift and lowest intensity in the more polar environment ($\sim 40\%$ dioxane); and iii) as the solvent polarity increased to $>40\%$ dioxane, DChol showed increased polarization and light scattering, consistent with the low critical micelle/microcrystalline concentrations exhibited by both cholesterol and fluorescent sterol analogs in aqueous buffers (15, 16, 42).

DChol in LUV model membranes

To determine the apparent polarity of the microenvironment sensed by DChol in a membrane lipid bilayer independent of the presence of proteins, DChol fluorescence spectra were obtained in a model membrane system (LUV) comprised of POPC:total sterol = 65:35, with DChol accounting for 1% of total sterol. Comparison with DChol Stokes shift of 186 in LUV with that in solvent of different polarity (Fig. 1D) indicated the polarity of the microenvironment sensed by DChol in lipid LUV was near a dielectric constant of 15.

To determine the structural order of the cholesterol microenvironment sensed by DChol in a membrane lipid bilayer environment, DChol polarization was measured in the above LUV. The polarization of DChol in the LUV membrane lipid environment was 0.2, nearly 2-fold higher than for DChol localized in micelles (Fig. 1G). This suggested that the DChol either exhibited 2-fold higher order in the lipid environment of LUV than in DChol micelles/microcrystals, or DChol was self-quenched in micelles, which resulted in decreased polarization as compared with DChol in LUV.

Experiments were carried out to determine if DChol experienced self-quenching in lipid bilayer. When the percentage of DChol in the total sterol in LUVs was increased from 0.5 to 10%, fluorescence intensity of DChol in LUV increased linearly (Fig. 1I), and DChol polarization did not change significantly (Fig. 1J). These results indicated

that when DChol comprised up to 10% of total sterol in lipid bilayer, there was very little if any DChol self-quenching and DChol did not cause any disruption of membrane structure.

DChol metabolism in L-cell fibroblasts

M β CD was used as a vehicle to facilitate DChol uptake by L-cells, because cholesterol and DChol are poorly soluble in aqueous buffer. One of the advantages of using M β CD complex is that once the complex is formed, cholesterol and DChol will not precipitate out of the solution upon dilution. It was reported previously that cholesterol binds 2-hydroxypropyl- β -cyclodextrin with the dissociation constant = 1.5 mM, an affinity sufficiently weak to thereby make the cholesterol cyclodextrin complex an excellent cholesterol donor (43). The dissociation constants of M β CD were determined to be 1.3 mM and 2.0 mM for cholesterol and DChol, respectively (supplementary Fig. II). Therefore, M β CD showed similarly weak affinity for both cholesterol and DChol.

DChol metabolism in L-cells was studied. After 30 min incubation with DChol-M β CD, none of the DChol taken up by L-cells was esterified (Table 1). If at the end of 30 min incubation, the DChol-M β CD complex was removed and cells were incubated with serum containing medium without DChol, then 5.4% and 19.4% of DChol taken up were esterified after 3 and 24 h, respectively (Table 1). The pattern of fatty acids esterified to DChol was very similar to that of cholesterol esters (not shown). Because total DChol uptake (3.6 and 2.8 nmol/mg protein, respectively) after 3 h or 24 h incubation with DChol free medium was not substantially different from that of cells incubated for only 30 min with DChol (2.7 nmol/mg protein), the DChol taken up was not degraded by the L-cell fibroblasts. Finally, when cells were incubated with DChol-M β CD complex continuously overnight (24 h), total uptake of DChol was 3.2-fold greater than the 30 min pulse incubation and about 4% of the DChol was esterified (Table 1). In earlier studies, it was reported that 3.7% [¹H]cholesterol was esterified by L-cells after 24 h incubation, while 1.4–7.5-fold more NBD-cholesterol and DHE were esterified (29). Therefore, DChol was esterified similarly to cholesterol by L-cells, unlike NBD-cholesterol and DHE. In addition, the results suggested that incubating L-cells with DChol-M β CD for less than 30 min would allow real-

time imaging primarily of the unesterified form of DChol.

Incorporation of DChol into cholesterol-rich and -poor fractions resolved by affinity chromatography of purified plasma membranes from L-cell fibroblasts

Plasma membranes of eukaryotic cells are not homogeneous but are instead comprised of distinct lateral microdomains termed cholesterol-rich and -poor microdomains (3, 4, 6). Because cholesterol-rich microdomains isolated biochemically are enriched in cholesterol (6), the distribution of DChol in cholesterol-rich and -poor microdomains was compared with that of cholesterol.

When L-cells were incubated with DChol-M β CD complex, the distribution of DChol taken up into cholesterol-rich vs. -poor microdomains was highly dependent on incubation time (Table 2). On a mass basis, after 15 min incubation, cholesterol-rich microdomains were enriched 2.1-fold in DChol compared with cholesterol-poor microdomains. This is similar to cholesterol, which was reported to be enriched 2.5-fold in the cholesterol-rich microdomains compared with cholesterol-poor microdomains on a mass basis (22). When compared on a percent of total sterol basis, DChol comprised essentially the same low percentage of total sterol in cholesterol-rich and -poor microdomains, indicating that DChol codistributed with cholesterol in both cholesterol-rich and -poor microdomains. In contrast, at longer incubation times, larger amounts of DChol (0.5–2.4% of total sterol) were incorporated into the plasma membrane and DChol was increasingly distributed into cholesterol-poor microdomains (Table 2).

DChol detects the polarity and structure of sterol in affinity purified cholesterol-rich and -poor microdomain-enriched fractions resolved from isolated L-cell plasma membranes

Because DChol was sensitive to polarity and order/structure in solvents and model membranes, these properties of DChol were examined in affinity-purified cholesterol-rich and -poor microdomains from L-cells incubated for 15 min with DChol-M β CD. Comparison of Stokes shift of DChol in cholesterol-rich and -poor microdomains (Table 3) with those in solvents (Fig. 1D) allowed estimation of the relative dielectric constants of the microenvironment sensed by the dansyl group in DChol in these plasma membrane microdomains to be near 18. The results suggested that the polarity of the microenvironment sensed by DChol was the same in both cholesterol-rich and -poor membrane domains and that the dansyl group was located near the polar aqueous/membrane bilayer interface in both plasma membrane domains.

In contrast to the lack of difference in membrane microenvironment polarity sensed by DChol in cholesterol-rich and -poor microdomains, the fluorescence polarization of DChol differed markedly in these domains. The fluorescence polarization of DChol in the cholesterol-rich microdomain fraction was significantly lower than in the cholesterol-poor microdomain fraction (Table 3). Because DChol was not self-quenched when DChol comprised up

TABLE 1. DChol esterification in L-cell fibroblasts

Incubation Time		nmol/mg Protein		%	
With/Without DChol					
With (h)	Without (h)	DChol	Ester	DChol	Ester
0.5	0	2.7 ± 0.4	ND	100	0
0.5	3	3.4 ± 0.2	0.19 ± 0.01	94.6 ± 0.4	5.4 ± 0.4
0.5	24	2.3 ± 0.3	0.54 ± 0.05	80.6 ± 0.7	19.4 ± 0.7
24	0	8.6 ± 0.5	0.35 ± 0.02	96.1 ± 0.1	3.9 ± 0.1

L-cells were incubated with medium containing DChol-M β CD (20 μ g/ml). Cells were incubated for 30 min–24 h with DChol, followed by incubation without DChol for 0–24 h as indicated. Cells were then washed, lipid extracted and resolved by TLC, and DChol and DChol ester quantitated as described in Methods. ND: not detected. Values represent the mean \pm SEM, n = 4.

TABLE 2. Distribution of DChol in cholesterol-rich and -poor microdomains isolated from L-cell fibroblast plasma membranes by affinity chromatography

Incubation with DChol (h)	DChol (nmol/mg protein)		Ratio in Cholesterol-Rich/ Cholesterol-Poor Microdomains	% Chol Replaced by DChol	
	Cholesterol-Rich Microdomains	Cholesterol-Poor Microdomains		Cholesterol-Rich Microdomains	Cholesterol-Poor Microdomains
0.25	2.06 ± 0.69	0.98 ± 0.58	2.10 ± 0.84	0.21 ± 0.07	0.25 ± 0.15
1	4.52 ± 0.90	4.53 ± 0.18	0.99 ± 0.16	0.46 ± 0.09	1.16 ± 0.05
24	7.10 ± 0.65	9.37 ± 0.25	0.76 ± 0.04	0.72 ± 0.05	2.4 ± 0.06

L-cells were incubated with DChol-M β CD complex (20 μ g/ml medium) for the indicated times as described in Methods. Cells were then fractionated to isolate plasma membranes, which were in turn resolved into cholesterol-rich and -poor microdomain enriched fractions by affinity chromatography, lipids were extracted, and DChol and cholesterol were quantitated as described in Methods. Values represent mean \pm SEM of two experiments.

to 10% of total membrane sterol (Fig. 1I), DChol representing 0.2% of total sterol in cholesterol-rich and -poor microdomains was not self-quenched. Therefore, the lower polarization indicated that DChol sensed a more fluid microenvironment in cholesterol-rich than -poor microdomains near the polar aqueous/membrane bilayer interface.

Real-time distribution of DChol in the plasma membrane of living cells: qualitative colocalization with cholesterol-rich and -poor specific microdomain markers

To determine if DChol preferentially distributed to cholesterol-rich microdomains in the plasma membrane of living cells, L-cells were double labeled with DChol and another membrane domain marker and their colocalization images (Fig. 2) were obtained as described in Methods. Although DChol (like cholesterol) is qualitatively distributed in both cholesterol-rich and -poor microdomains, quantitative analysis of the distribution was expected to reveal preferential distribution into cholesterol-rich microdomains.

DChol colocalization with cholesterol-rich microdomain marker GM₁. L-cells were preincubated with Alexa Fluor 594-cholera toxin B (Alexa Fluor 594 CT-B), which directly binds to GM₁, a known marker of cholesterol-rich microdomains (6, 22, 26). Cells were then further incubated with DChol-M β CD Complex (DChol), followed by simultaneous imaging of DChol (Fig. 2B) and Alexa Fluor 594 CT-B (Fig. 2A) in real time by LSCM through two separate photomultipliers, as described in Methods. Alexa Fluor

594 CT-B distributed most intensely at the cell surface plasma membrane, but not uniformly (Fig. 2A). DChol also distributed at the plasma membrane (Fig. 2B) into regions with high and low fluorescence intensity. Superposition of these simultaneously acquired images and qualitative comparison showed many pixels that were neither red (Alexa Fluor 594 CT-B) nor green (DChol) but were intermediate in color, suggesting colocalization (Fig. 2C). Indeed, when only the colocalized yellow pixels were displayed (Fig. 2D), it was apparent that DChol significantly colocalized with Alexa Fluor 594 bound to GM₁ at the plasma membrane and this distribution was not uniform. Plotting the ratio of DChol distribution in cholesterol-rich regions (colocalized with Alexa Fluor CT-B)/cholesterol-poor regions (not colocalized with Alexa Fluor CT-B) showed that at earlier time point, DChol preferentially distributed to cholesterol-rich microdomains than at later time points (Fig. 2Q). The imaging results agreed with the results obtained from biochemical fractionation shown above.

DChol colocalization with the cholesterol-rich microdomain liquid ordered phase marker DiD. Because cholesterol-rich microdomains are more liquid ordered than cholesterol-poor microdomains, it was important to determine if DChol also colocalized with a fluorescence probe DiD, a probe preferentially localized to liquid ordered phase (44, 45). DiD distribution in the plasma membrane was nonuniform, displaying a patchy pattern with strong fluorescent areas and weak fluorescent areas (Fig. 2E). DChol distribution in the plasma membrane (Fig. 2F) exhibited a very similar pattern to that of DiD, as shown by colocalization (Fig. 2G) and display of only colocalized pixels (Fig. 2H, yellow pixels). To quantitatively determine the relative DChol distribution between cholesterol-rich and -poor microdomains, the fluorescence intensities of DChol colocalized with as well as those not colocalized with DiD were determined and the ratio in cholesterol-rich-cholesterol-poor microdomains was plotted for the first 20 min (Fig. 2R). The results clearly showed that at earlier time points, DChol preferentially distributed to cholesterol-rich microdomains.

DChol colocalization with cholesterol-rich microdomain marker BC θ . BC θ , the nonlytic fragment of a bacterial cytolysin, has high affinity for cholesterol in cholesterol-rich microdomains (46). Alexa Fluor 660 BC θ was distributed non-

TABLE 3. Polarity and polarization of DChol in cholesterol-rich and -poor microdomains resolved from plasma membranes isolated from L-cell fibroblasts

Parameter	Cholesterol-Rich Microdomains	Cholesterol-Poor Microdomains
Excitation Maximum (nm)	332 ± 1	331 ± 1
Emission Maximum (nm)	520 ± 1	521 ± 2
Stokes shift (nm)	188 ± 1	190 ± 2
Polarization	0.203 ± 0.005	0.244 ± 0.002

L-cells were incubated with DChol-M β CD complex (20 μ g/ml medium) for 15 min as described in Methods. Cells were then fractionated to isolate plasma membranes, plasma membranes were resolved into cholesterol-rich and -poor microdomain enriched fractions by affinity chromatography, and fluorescence parameters were determined as described in Methods. Values represent the mean \pm SEM (n = 3–10).

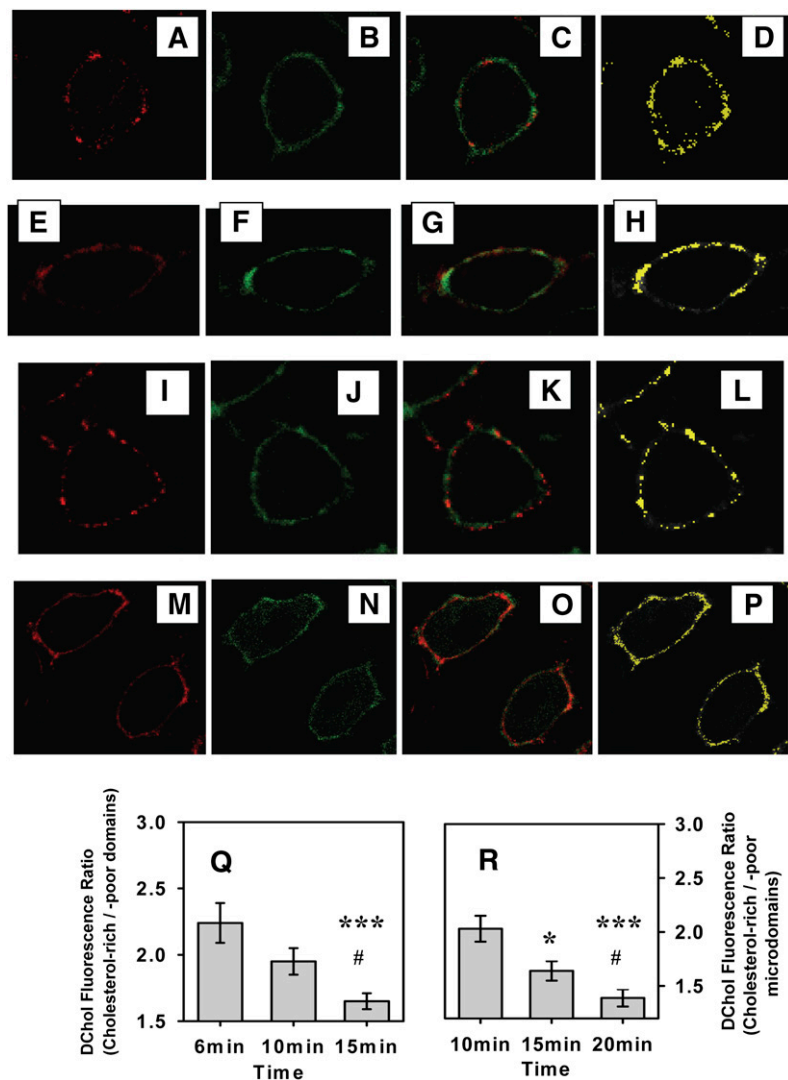


Fig. 2. Colocalization of DChol with different microdomain markers in living cells. L-cells were double labeled with DChol and another membrane domain marker, which were then simultaneously imaged through separate photomultipliers as described in Methods. Images of DChol are shown in green in B, F, J, and N. The images of membrane domain markers are shown in red: Alexa Fluor 594 CT-B (A), DiD (E), BC θ (I), and N-Rh-DOPE (M). The superposition of red and green images are shown in C, G, K, and O, and the yellow colocalized pixels are shown in D, H, L, and P. Changes in DChol uptake into cholesterol-rich and -poor microdomains with time were followed by measuring the ratio dansyl fluorescence (cholesterol-rich/-poor microdomains) with time based on DChol colocalization with Alexa Fluor 594 CT-B as shown in Q. ***, Significantly different from 6 min ($P < 0.001$); #, significantly different from 10 min ($P < 0.05$). R: DChol fluorescence distribution (cholesterol-rich/-poor microdomains) with time based on colocalization with DiD. *, Significantly different from 10 min ($P < 0.05$), ***, $P < 0.001$); #, significantly different from 15 min ($P < 0.05$).

randomly at the surface plasma membrane of cultured L-cell fibroblasts (Fig. 2I). DChol was highly colocalized with BC θ as shown by superposition of DChol (Fig. 2J) and BC θ (Fig. 2I) images to yield a superposed image (Fig. 2K). Display of only colocalized pixels showed that DChol/BC θ colocalized pixels were distributed in a clustered pattern at the plasma membrane (Fig. 2L).

Colocalization between DChol and the cholesterol-poor microdomain marker N-Rh-DOPE. N-Rh-DOPE, which contains two unsaturated acyl chains, is known to preferentially distribute to fluid or liquid disordered phase in lipid bilayers (47, 48). Because cholesterol-poor as well as cholesterol-rich microdomains contain DChol, confocal imaging (Fig. 2M–P) also detected regions in the PM where Rh-DOPE and DChol colocalized.

Real-time distribution of DChol in the plasma membrane of living cells: quantitative analysis of colocalization with cholesterol-rich and -poor specific microdomain markers

Confocal colocalization images showed that DChol colocalized to some degree with all the membrane probes tested regardless of whether the probes were cholesterol-

rich or -poor domain probes. This was not unexpected, because both types of microdomains contain cholesterol, albeit at different concentrations. Therefore, quantitative colocalization analysis was performed with three independent procedures (supplementary Method IV) to determine whether the observed colocalizations were significantly different from each other and from that by chance alone.

Mander's colocalization coefficients. Mander's colocalization coefficients, M_{red} and M_{green} , were calculated for each pair of probes. For DHE, DiD, CT-B, and BC θ , M_{red} showed that about 50–60% of their fluorescence intensities were colocalized with DChol; in contrast, <30% of the N-Rh-DOPE fluorescence was colocalized with DChol (Table 4). M_{green} showed higher percentages of DChol fluorescence colocalization with DHE (56%) and DiD (50%) and lower percentages of DChol fluorescence colocalization with CT-B, BC θ , and N-Rh-DOPE (Table 4). The percentages of colored pixels (data not shown) were calculated for each probe to determine the degree of labeling. The results indicated that the percentages of DChol labeling were relatively stable regardless of the second probe used.

Therefore, the difference in M_{red} indicated that DHE, DiD, CT-B, and BC θ had a higher tendency to colocalize with DChol than N-Rh-DOPE. In contrast, the abundance and/or degree of labeling varied greatly between these different membrane markers (data not shown) in the order of DHE \approx DiD \approx N-Rh-DOPE $>$ CT-B \approx BC θ . Therefore, as shown in Table 4, even though M_{green} showed different degrees of colocalization of DChol with the other probes, the differences in M_{green} could be due to differences in colocalization tendency or due to differences in the availability of the other probe. To resolve this issue and determine if the observed colocalization was significant and not just due to chance, the observed colocalizations were compared with the colocalizations predicted for a random distribution as described below.

Costes randomization test. Image J with Colocalization Test plugin was used to create 200 randomized DChol images by scrambling DChol fluorescent pixels within the plasma membrane regions of interest. Then Pearson's correlation coefficient for the two channels (R_{obs}) was calculated and compared with the Pearson's coefficients for red channel against the randomized DChol channel images (R_{rand}). For DChol colocalization with DHE, DiD, CT-B, and BC θ , $R_{obs} > R_{rand}$ 100% of time (Table 4), indicating the observed colocalizations between DChol and these probes were significantly more than if due to random chance. For DChol colocalization with N-Rh-DOPE, calculations revealed that $R_{obs} < R_{rand}$ 100% of time (Table 4), indicating a greater tendency for exclusion.

Ratio of observed-random colocalizing pixels. The ratios of the observed percentages of colocalizing pixels to the predicted percentages using a random distribution of the peak intensities were calculated for each pair of fluorescent probes. The results, tabulated in Table 4, showed the

TABLE 4. Comparison of DChol (green) colocalization with different fluorescent membrane markers (red)

Fluorescent PM Markers	Colocalization Coefficients			
	Mander's		Costes	Observed/Random Ratio (mean \pm SE)
	M_{red}	M_{green}	Randomization (N = 200) % ($R_{obs} > R_{rand}$)	
DHE (n = 22)	0.61	0.56	100%	2.28 \pm 0.08 **, #
DiD (n = 23)	0.51	0.50	100%	1.93 \pm 0.14 *, ##
Alexa Fluor CT-B (n = 26)	0.59	0.30	100%	2.19 \pm 0.13 **, #
BC- θ (n = 14)	0.59	0.27	100%	2.69 \pm 0.21 **
N-Rh-DOPE (n = 16)	0.29	0.20	0%	1.49 \pm 0.10

DChol and a membrane domain probes were collected in two separate channels. The images were background corrected, threshold was set to select pixels with above average intensities, and regions of interests were drawn to include only the plasma membrane of each cell. Mander's colocalization coefficients M_{red} and M_{green} were calculated and Costes Randomization Test was performed with ImageJ using Colocalization Test plugin as described in supplementary Method IV. The observed/random ratio was the ratio of the observed percentage of colocalized pixels to the predicted percentage of colocalized pixels assuming a random distribution of both probes. *, **, Significantly different from that of N-Rh-DOPE; #, ##, significantly different from that of BC θ ; *, #, $P < 0.05$; **, ##, $P < 0.01$.

following: *i*) ratios for all the pairs were higher than 1, suggesting higher colocalization than random distribution; *ii*) the ratios for DChol colocalization with DHE, DiD, CT-B, and BC θ were significantly higher than that for N-Rh-DOPE, indicating DHE, DiD, CT-B, and BC θ had a higher preference for colocalization with DChol than N-Rh-DOPE; *iii*) the ratio for BC θ , a marker for cholesterol-rich microdomains, was significantly higher than the ratios for DHE, DiD, and CT-B, indicating BC θ had the highest preference for colocalization with DChol.

Taken together, the above quantitative analyses of colocalization data were consistent with DChol residing in both cholesterol-rich and -poor microdomains but preferentially distributing to cholesterol-rich microdomains in plasma membranes of living L-cell fibroblasts.

FRET to determine intermolecular distance between DChol and cholesterol-rich or -poor microdomain markers

Resolution of confocal imaging is $>2,000$ Å and some microdomains may be much smaller (3, 4, 6, 14, 16, 38, 49). Therefore, FRET experiments were performed to determine if DChol and the membrane probes were in proximity to allow fluorescence energy transfer. The limit of resolution of FRET is in the range of 10–100 Å (depending on the donor/acceptor pair) (50), well within the range of small microdomains (3, 4, 6, 14, 16, 38, 49).

FRET between DChol (acceptor) and the cholesterol-rich microdomain marker DHE (donor) in model membranes (LUVs). When acceptor DChol content increased from 0 to 10%, donor DHE emission decreased, while the emission of acceptor DChol increased (Fig. 3A), indicating energy transfer from donor DHE to acceptor DChol. The energy transfer efficiency was calculated and shown as a function of DChol content (Fig. 3B, open circles). At 10% (mol%) DChol, the energy transfer efficiency was about 70%.

Next, the predicted energy transfer efficiency using a mathematical model of DChol randomly codistributed with DHE in the LUV was calculated. The Förster distance using the typical dynamical averaged value of $\kappa^2 = 2/3$ was found to be $R_0 = 15.5$ Å. By implication, two probes would have to be fairly close for a FRET interaction, as could be the case if the two probes codistributed in lipid membrane bilayers. Because the orientation factor of κ^2 can range between 0 and 4 depending upon the orientational freedom of the donor and acceptor involved in FRET (51), the range was further narrowed by experimental techniques to determine the upper and lower bounds for κ^2 . Time-resolved measurements of anisotropy parameters were made using donor LUVs containing 5 mol% DHE and acceptor LUVs containing 10 mol% DChol in 2 ml PBS (see supplementary Method VI). The two rotational times for DHE and DChol, the fractional anisotropies, and, subsequently, the limiting anisotropy of each probe, were used to calculate the depolarization factors of DHE and DChol (Table 5). The minimum and maximum values of the orientation factor for donor-acceptor resonance interaction yielded the upper and lower limits on the Förster distance,

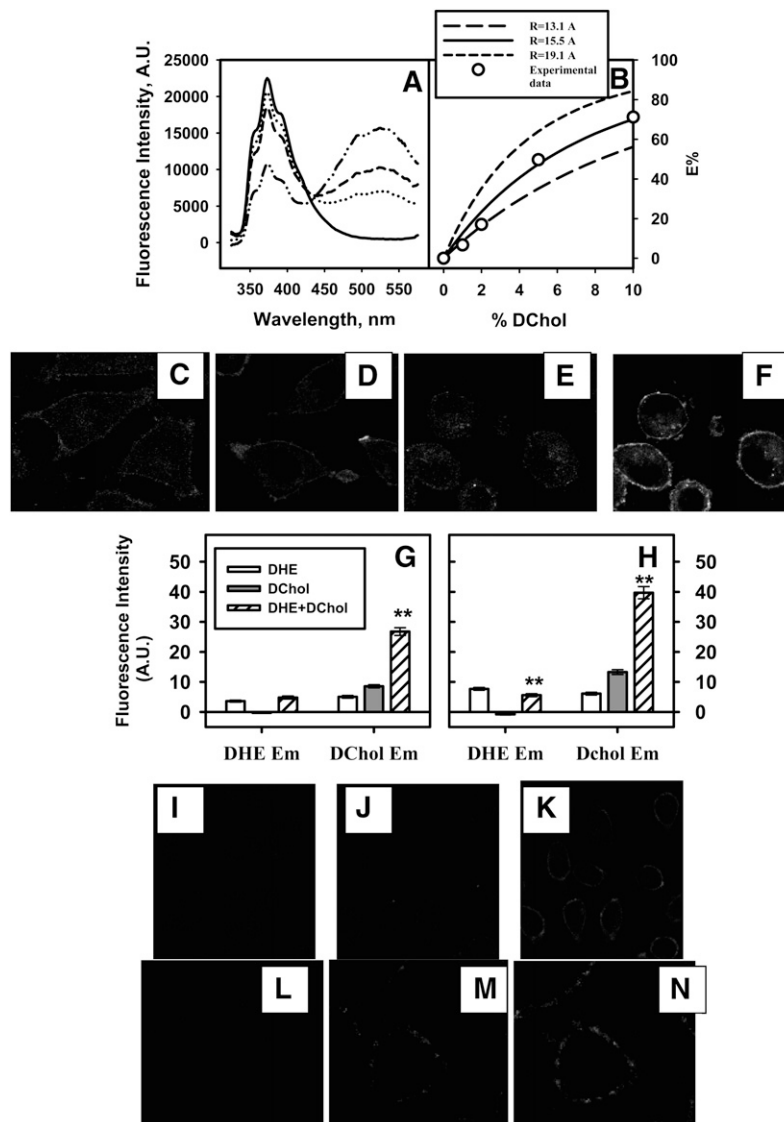


Fig. 3. FRET between DChol and cholesterol-rich microdomain markers DHE, DiD, and BC θ . A and B: FRET between DChol and DHE in LUVs. A: Emission spectra (325–575 nm) of LUVs containing 5% DHE and increasing amount of DChol. The spectra were recorded at 37°C with 300 nm excitation. B: The energy transfer efficiency E% as a function of increasing DChol (mol%). Open circles, E% was calculated from experimental data by $E = 1 - I_{DA}/I_D$, where I_{DA} and I_D were donor DHE fluorescence intensity at 373 nm in the presence and absence of acceptor DChol, respectively; lines, E% was calculated using a mathematical model of random distribution of DChol relative to DHE in LUV bilayer as described in Methods. Solid line, $R = 15.5$; short dashed line, $R = 19.1$; long dashed line, $R = 13.1$. C–H: FRET between DChol and DHE in living cells by multi-photon imaging. Images were taken with multi-photon excitation using a 900 nm laser and a D375/50 (350–400 nm) emission filter for DHE (C, E), BGG22 (410–490 nm) emission filter for DChol (D, F). C: DHE emission when L-cells were incubated with DHE only. D: DChol emission when L-cells were incubated with DChol only. E: DHE emission when L-cells were incubated with both DHE and DChol. F: DChol emission when L-cells were incubated with both DHE and DChol. G: Average fluorescence intensity of whole cells (mean \pm SE, $n = 16$ –24). H: Average fluorescence intensity of PM (mean \pm SE, $n = 16$ –24). **, $P < 0.01$ *t*-test, significantly different from DHE only for DHE emission and significantly different from DChol only for DChol emission. FRET between DChol and DiD (I–K) and BC θ (L–N). The excitation laser 408 nm was chosen to only excite the donor DChol and emission filter 680/32 was used to only detect the emission from acceptor DiD and BC θ . Upper panels show FRET between DChol (donor) and DiD (acceptor). I: Image of cells labeled with donor DChol only. J: Image of cells labeled with acceptor DiD only. K: Cells were labeled with both DChol and DiD. Lower panels show FRET between DChol (donor) and Alexa Fluor 660 BC θ (acceptor). L: DChol only. M: Alexa Fluor 660 BC θ only. N: DChol plus Alexa Fluor 660 BC θ .

R_{min} and R_{max} . Due to the uncertainty in the orientation factor, the curves (Fig. 3B) show the possible range of FRET efficiencies as a function of DChol% (mol%) for a random distribution of DChol about DHE in the model membranes.

FRET Between DChol (acceptor) and cholesterol-rich microdomain marker DHE (donor) in plasma membranes of living cells. To show if DChol and DHE were also codistributed in proximity in plasma membranes of living cells, FRET between DChol (acceptor) and DHE (donor) was performed by multiphoton laser scanning microscopy. When cells were incubated with only DHE, DHE emission was prominently detected at the plasma membrane in a visually nonrandom pattern but less intensely within the cells (Fig. 3C). A similar pattern was observed when cells were incubated only with DChol and DChol emission was observed (Fig. 3D). However, when L-cells were incubated with both DHE (FRET donor) and DChol (FRET acceptor), the emission of the DHE donor was weaker, especially at the plasma membrane but still in a nonrandom pattern (Fig. 3E). Concomitantly, emission of the acceptor DChol was increased, especially at the plasma membrane in a nonrandom pattern (Fig. 3F). Quantitative FRET analysis of whole cells (Fig. 3G) and plasma membranes (Fig. 3H) revealed the DChol emission was significantly increased several-fold. The results indicated that in living L-cells, the DChol and DHE were also codistributed in proximity. Further, the FRET pattern at the plasma membrane was not uniformly distributed along the plasma membrane but instead appeared clustered into bright and less intense regions consistent with microdomains rich or poor in DChol and DHE.

FRET between DChol (donor) and cholesterol-rich liquid-ordered microdomain marker DiD (acceptor) in plasma membranes of living cells. FRET was carried out by exciting the donor DChol with a 408 nm laser and observing the emission of acceptor DiD with a 680/32 filter. When cells were labeled with donor DChol only, no fluorescence signal was detected (Fig. 3I), because the emission filter blocked out donor DChol emission. When cells were labeled with only DiD, no fluorescence emission signal was observed (Fig. 3J), because DiD does not absorb at 408 nm. When cells were labeled with both DChol as well as DiD and then excited at 408 nm (excites only donor DChol), the fluorescence emission of acceptor DiD was clearly observed (Fig.

3K), indicating DiD and DChol were in proximity to permit energy transfer from DChol to DiD.

FRET between DChol (donor) and cholesterol-rich microdomain marker BCθ (acceptor) in plasma membranes of living cells. BCθ, the nonlytic fragment of a bacterial cytolysin, has high affinity for cholesterol in cholesterol-rich microdomains (46). FRET was performed to excite donor DChol (408 nm laser at 30% power) and detect acceptor Alexa Fluor 660 BCθ emission. When DChol and Alexa Fluor 660 BCθ were both present and donor DChol was excited, the acceptor emission appeared brighter (Fig. 3N) compared with when only the acceptor was present (Fig. 3M). The increase in fluorescence was not due to emission from donor DChol, because when only DChol was present, no emission signal was detected (Fig. 3L).

Lack of FRET between DChol (donor) and cholesterol-poor microdomain marker N-Rh-DOPE (acceptor) in plasma membranes of living cells. FRET experiments were carried out to investigate if N-Rh-DOPE and DChol were in close proximity to permit fluorescence energy transfer. First, when donor DChol was excited at 408 nm, there was no significant increase in acceptor emission or significant decrease in donor emission (data not shown). Second, when N-Rh-DOPE acceptor was photobleached with 100% laser power at 568 nm for 6 min, there was no significant change in DChol donor emission compared with DChol donor emission before acceptor photobleaching. As a control experiment, when cells labeled with DChol only were subjected to the same photobleaching procedure, DChol fluorescence emission was not altered. Therefore, donor emission, acceptor emission, and acceptor photobleaching experiments all showed no significant FRET between DChol and Rh-DOPE.

In summary, FRET experiments demonstrated that DChol was very close (10–100 Å) to cholesterol-rich liquid-ordered microdomain markers (DHE, DiD, BCθ) but not cholesterol-poor microdomain markers (N-Rh-DOPE) in the plasma membrane of living cells.

Real-time confocal imaging of DChol trafficking through plasma membrane cholesterol-rich and -poor microdomains of living cells: DChol uptake from DChol/MβCD

DChol uptake from DChol-MβCD was examined in real time by LSCM of living L-cell fibroblasts. Uptake into

TABLE 5. Time-resolved anisotropy parameters, FRET orientation factor κ^2 , and Förster distance for DHE and DChol in LUVs

Fluorophore	r_1	θ_1 (ns)	r_2	θ_2 (ns)	r_0
DHE	0.098 ± 0.001	0.39 ± 0.03	0.204 ± 0.003	13.8 ± 0.4	0.302 ± 0.003
DChol	0.05 ± 0.01	3.1 ± 0.5	0.08 ± 0.01	23 ± 2	0.134 ± 0.009
	d_i^x	κ^2_{min}	κ^2_{max}	R_{min}	R_{max}
DHE	0.68 ± 0.01	0.24 ± 0.03	2.3 ± 0.4	$13.1 \pm 0.3 \text{ \AA}$	$19.1 \pm 0.6 \text{ \AA}$
DChol	0.60 ± 0.08				

Time-resolved anisotropy parameters (fractional anisotropies r_i , rotational correlation times, θ_i , and limiting anisotropy, r_0) for DHE and DChol in LUVs were measured as described in Methods. From these parameters, depolarization factor (d_i^x), upper and lower limits on the FRET orientation factor κ^2 , and Förster distance (R) were calculated, as described in Methods.

whole cells, plasma membranes, and intracellular regions was monitored as described in Methods. DChol uptake into control whole cells was rapid, detectable at the earliest time points measured, and did not plateau even by 14 min (Fig. 4A, solid circles). The uptake kinetics into the plasma membrane (Fig. 4A, solid inverted triangles) was faster, whereas that into the intracellular regions (Fig. 4A, solid squares) was slower compared with uptake into the whole cell (Fig. 4A, solid circles). DChol uptake into cholesterol-rich and -poor microdomains was estimated from DChol fluorescence measurement of pixels that were colocalized (Fig. 4B, solid triangles) and not colocalized (Fig. 4B, open triangles) with Alexa Fluor 594 CT-B, respectively, at the plasma membrane. For the first 15 min, DChol distribution into cholesterol-rich microdomains was significantly faster than into cholesterol-poor microdomains. These were consistent with the results from con-A affinity column isolation of cholesterol-rich and -poor fractions, which also showed DChol preferentially distributed to cholesterol-rich domain at shorter incubation times.

DISCUSSION

Plasma membrane cholesterol-rich microdomains are rich in cholesterol and liquid ordered phase compared with cholesterol-poor microdomains (3, 5, 6, 22, 26, 49, 52–54). Despite the more ‘rigid’ environment of cholesterol-rich microdomains, experiments performed *in vitro* with purified cholesterol-rich and -poor microdomains show that cholesterol transfers into and out of cholesterol-rich microdomains much more rapidly than into/out of

cholesterol-poor microdomains (6, 22, 26, 52, 53). While these *in vitro* studies suggest that cholesterol may reside in a significantly different microenvironment in cholesterol-rich than -poor microdomains, the significance of these *in vitro* studies of plasma membranes to living cells has not been established. These issues were addressed herein by use of DChol, model membrane system, affinity purification of cholesterol-rich and -poor microdomains, and real-time imaging of DChol in cultured L-cell fibroblasts to yield the following new insights.

DChol was oriented similarly to cholesterol in membrane bilayer as shown by polarity sensitivity. The polarity sensed by DChol in model membrane bilayer correlated with a dielectric near 15 very similar to that sensed by dansyl attached to the polar head group of dansyl-phosphatidylethanolamine in model membrane bilayer, which correlated with a dielectric near 19 (40). This suggests the dansyl group in DChol resides closer to the surface rather than deep toward the center of the bilayer.

Because naturally occurring fluorescent sterol DHE is known to orient similarly and codistribute with cholesterol in cholesterol-rich and -poor microdomains (14–16, 37, 38), FRET between DHE and DChol was used to determine if DChol oriented and codistributed in proximity similarly to DHE and, by extension, thereby similarly to cholesterol. A mathematical model of DChol randomly codistributed with DHE in the LUV was used to predict energy transfer efficiency and then compared with the experimental data. In this model, changes in external radii (r_e) while maintaining a constant interaction thickness involved had little effect on the resultant FRET efficiency. However, changes in the interaction distances along the

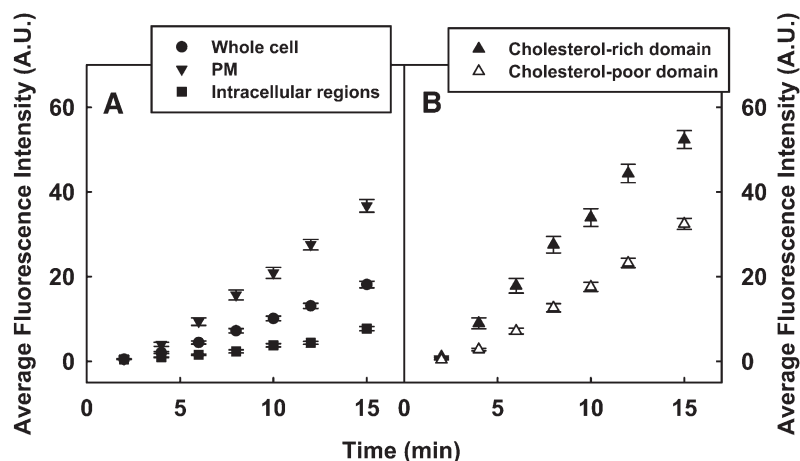


Fig. 4. Real-time confocal imaging of DChol uptake through cholesterol-rich and -poor microdomains of L-cell fibroblasts. Cells were first labeled with Alexa Fluor CT-B as described in Methods, then DChol-M β CD (DChol concentration 10 μ g/ml) was added to the cells in PBS and fluorescence images were acquired continuously for the first 15 min at room temperature. A: Average DChol fluorescence in the whole cell (solid circles), in the plasma membrane (PM, solid inverted triangles), and intracellular regions (solid squares). B: Average DChol fluorescence in the PM that colocalized with the cholesterol-rich microdomain marker Alexa Fluor CT-B (solid triangles) and not colocalized with Alexa Fluor CT-B (open triangles). Images of DChol was obtained with 408 nm excitation and HQ530/40 emission filter, images of Alexa Fluor CT-B were obtained with 568 nm excitation and HQ598/40 emission filter. Data were presented as mean \pm SE (n = 25).

bilayer thickness might be important. It has been reported recently (55) that the top of the B ring of the steroid backbone of cholesterol resides 16 Å from the bilayer center in model membranes composed of 16:0-18:1 PC as measured using a [2,2,3,4,4,6-²H₆]labeled cholesterol in combination with neutron diffraction. This location would be within 2 Å from the relative center of the fluorescent DHE conjugated system similarly arranged as cholesterol within the bilayer. Subsequent calculations (not shown) using different bilayer thicknesses found that as a result of the short Förster distance between DHE and DChol ($R_0 = 15.5$ Å), the model was insensitive to any increases in the interaction distances along the bilayer depth ($\Delta r > 32$ Å) across the range of concentrations used in this experiment. However, the model became increasingly sensitive for substantial decreases in interaction depths ($\Delta r < 26$ Å), resulting in a significant increase in FRET efficiency compared with the calculation at $\Delta r = 32$ Å (Fig. 3B). Thus, the data are consistent for a random distribution of the DChol about the DHE with orientations of the fluorescently labeled sterols oriented with the hydroxyl group at the water-lipid interface as has been reported for cholesterol's polar head group (β -OH) orientation in POPC and most other model membrane bilayers (55). The only exception is the inverted (β -OH in center of bilayer) orientation of cholesterol in pure di-C22:6n-3PC/cholesterol bilayers (55). However, cholesterol-rich and -poor microdomains from plasma membranes of L-cells or other cells contain many different fatty acid species and only very low amounts of C22:6n-3, less in cholesterol-rich than -poor microdomains (22, 56, 57).

DChol fluorescence spectral and polarization data from isolated cholesterol-rich and -poor domain fractions showed that DChol sensed similar polarity but different fluidity between these two microdomains. Therefore, the faster spontaneous sterol transfer from cholesterol-rich microdomains observed *in vitro* (22, 26, 27, 52, 58) was not due to differences in exposure of cholesterol to the aqueous environment but to greater fluidity near the head group region in cholesterol-rich than in -poor microdomains. Spontaneous cholesterol transfer is known to be faster from more fluid membranes (2, 59). These findings were consistent with those of the naturally occurring fluorescent sterol DHE, which also exhibited lower polarization in cholesterol-rich than -poor microdomains isolated from L-cells (52). Interestingly, it should be noted that the bulk fatty acyl chain fluidity of L-cell plasma membrane cholesterol-rich microdomains was lower and more liquid ordered than in cholesterol-poor microdomains (6, 26, 52). This finding suggested that cholesterol may reside in a much more mobile region than the bulk lipid in the cholesterol-rich than -poor microdomains and that even though the interior (acyl chain region) of the phospholipid bilayer is more rigid, the region near the phospholipid polar head group is more fluid in cholesterol-rich than in -poor microdomains. In an analogous study, it was reported that the dansyl group attached to the polar head group in dansyl-phosphatidylethanolamine experienced decreased polarization in cholesterol-rich model membranes, suggesting

that while cholesterol increased the rigidity of the acyl chain region, it conversely increased the mobility/fluidity of the polar head group region (40). The localization of the dansyl group of DChol in a less ordered microenvironment in cholesterol-rich than -poor microdomains may account for the fact that cholesterol in cholesterol-rich microdomains exhibits faster and greater: i) spontaneous cholesterol trafficking (6, 22, 26, 52), ii) accessibility to cholesterol oxidase (8), iii) accessibility to the intracellular cholesterol transporter SCP-2 (6, 26, 36, 52), iv) direct interactions with caveolin-1, which is enriched in cholesterol-rich microdomains/caveolae, but not cholesterol-poor microdomains (60, 61), v) accessibility to plasma membrane cholesterol-rich microdomains/caveolae proteins involved in cholesterol uptake/efflux including caveolin-1, ABCA1 transporter, and SRB1 (62–64), and vi) accessibility to HDL and apoA1 (27, 63). These data suggest that not only the presence of reverse cholesterol transport proteins in cholesterol-rich microdomains and the expression of intracellular cholesterol binding proteins but also the structural properties of cholesterol therein play important role(s) in regulating cholesterol uptake/efflux.


Affinity chromatography of purified plasma membranes and real-time imaging of living L-cells indicate that at early time points of incubation, DChol was preferentially incorporated into plasma membrane cholesterol-rich microdomains. The findings fit either of two models: i) DChol was first taken up into cholesterol-rich microdomains and then diffused laterally into cholesterol-poor microdomains; or ii) DChol was taken up simultaneously into cholesterol-rich and -poor microdomains but at different rates. Studies with radiolabeled cholesterol and agents that disrupt cholesterol-rich microdomains favor the former possibility (7, 65, 66).

DChol showed intense colocalization with and participation in FRET with multiple cholesterol-rich microdomain markers. Confocal colocalization images showed that DChol colocalized to some degree with all the membrane probes tested regardless of whether the probes were cholesterol-rich or -poor domain probes. This was consistent with the fact that cholesterol distribution is not absolute but rather preferential, i.e., more in cholesterol-rich and less in cholesterol-poor microdomains (6, 14–16, 37). Results from additional quantitative colocalization analyses demonstrated that DChol preferentially distributed to cholesterol-rich compared with cholesterol-poor microdomains in the plasma membrane of living L-cell fibroblasts under nonsaturating conditions.

The FRET studies were particularly significant, because the limit of resolution of FRET (a few Å) is well within the size range of even the smallest cholesterol-rich microdomains (3, 6, 14–16, 37, 38, 49). Importantly, while efficient FRET was observed between DChol/DHE, DChol/BC θ , and DChol/DiD pairs, FRET did not occur between the DChol/Alexa Fluor CT-B pair (not shown). The latter observation served as a key negative control, because cross-linking studies with photoactivatable GM1 show that GM1 also does not cross-link with cholesterol

in cholesterol-rich microdomains (67). Furthermore, cholesterol is enriched in the cytofacial leaflet of L-cell plasma membranes, thereby making the intermolecular distance between DChol (enriched in cytofacial leaflet) and Alexa Fluor CT-B (exclusively at the exofacial leaflet) too great for efficient FRET (1, 68). Conversely, FRET between DChol and DiD was efficient, because DiD is preferentially distributed into more ordered lipids and the cytofacial leaflet is more ordered (2, 6, 26, 44, 45, 52, 69).

Kinetic analysis of real-time DChol uptake images indicated for the first time that DChol trafficked faster through cholesterol-rich than -poor microdomains of plasma membranes in living cells. These findings were consistent with earlier studies performed in vitro with purified cholesterol-rich and -poor microdomains isolated from plasma membranes of L-cell fibroblasts or cultured primary hepatocytes (22, 26, 52, 53). The molecular basis for faster DChol uptake via cholesterol-rich microdomains is not completely clear. In the case of L-cell fibroblasts, plasma membrane cholesterol-rich microdomains are rich in caveolin-1 and SRB-1, proteins known to facilitate cholesterol trafficking (7, 22, 27, 60, 61, 70). Although hepatocyte plasma membranes are relatively deficient in caveolin-1 (56), they nevertheless contain several other proteins that facilitate cholesterol trafficking through the plasma membrane (SRB1, P-gp, ABCG1, ABCA1) (6, 10). SRB1, P-gp, ABCG1, and likely ABCA1 at the plasma membrane are selectively localized in cholesterol-rich microdomains (6, 10, 56).

Taken together, the above findings indicated that DChol was a useful probe of cholesterol-rich and -poor microdomains with preferential selectivity for cholesterol-rich microdomains at early incubation times. 

The helpful technical assistance of Ms. Kerstin Landrock was much appreciated.

REFERENCES

- Schroeder, F., and G. Nemezc. 1990. Transmembrane cholesterol distribution. In *Advances in Cholesterol Research*. M. Esfahami, and J. Swaney, editors. Telford Press, Caldwell, NJ. 47–87.
- Schroeder, F., A. A. Frolov, E. J. Murphy, B. P. Atshaves, J. R. Jefferson, L. Pu, W. G. Wood, W. B. Foxworth, and A. B. Kier. 1996. Recent advances in membrane cholesterol domain dynamics and intracellular cholesterol trafficking. *Proc. Soc. Exp. Biol. Med.* **213**: 150–177.
- Pike, L. J. 2004. Lipid rafts: heterogeneity on the high seas. *Biochem. J.* **378**: 281–292.
- Pike, L. J. 2006. Rafts defined: a report on the Keystone symposium on lipid rafts and cell function. *J. Lipid Res.* **47**: 1597–1598.
- Brown, D. A., and E. London. 2000. Structure and function of sphingolipid- and cholesterol-rich membrane rafts. *J. Biol. Chem.* **275**: 17221–17224.
- Schroeder, F., B. P. Atshaves, A. M. Gallegos, A. L. McIntosh, J. C. Liu, A. B. Kier, H. Huang, and J. M. Ball. 2005. Lipid rafts and caveolae organization. In *Advances in Molecular and Cell Biology*. P. G. Frank and M. P. Lisanti, editors. Elsevier, Amsterdam. 3–36.
- Everson, W. V., and E. J. and Smart. 2005. Caveolae and the regulation of cellular cholesterol homeostasis. In *Caveolae and Lipid Rafts: Roles in Signal Transduction and the Pathogenesis of Human Disease*. M. P. Lisanti and P. G. Frank, editors. Elsevier Academic Press, San Diego. 37–55.
- Parathath, S., M. A. Connelly, R. A. Rieger, S. M. Klein, N. A. Abumrad, M. de la Llera-Moya, C. R. Iden, G. H. Rothblat, and D. L. Williams. 2004. Changes in plasma membrane properties and phosphatidylcholine subspecies of insect Sf9 cells due to expression of scavenger receptor class B, type 1, and CD36. *J. Biol. Chem.* **279**: 41310–41318.
- Connelly, M. A., and D. L. Williams. 2004. Scavenger receptor B1: a scavenger receptor with a mission to transport high density lipoprotein lipids. *Curr. Opin. Lipidol.* **15**: 287–295.
- Yancey, P. G., A. E. Bortnick, G. Kellner-Weibel, M. de la Llera-Moya, M. C. Phillips, and G. H. Rothblat. 2003. Importance of different pathways of cellular cholesterol efflux. *Arterioscler. Thromb. Vasc. Biol.* **23**: 712–719.
- Ortegren, U., M. Karlsson, N. Blazic, M. Blomqvist, F. H. Nysrom, J. Gustavsson, P. Fredman, and P. Stralfors. 2004. Lipids and glycosphingolipids in caveolae and surrounding plasma membrane of primary rat adipocytes. *Eur. J. Biochem.* **271**: 2028–2036.
- Saltiel, A. R., and J. E. Pessin. 2003. Insulin signaling in microdomains of the plasma membrane. *Traffic.* **4**: 711–716.
- Ikonen, E., and S. Vainio. 2005. Lipid microdomains and insulin resistance: is there a connection? *Sci.STKE* **pe3**:1–3.
- McIntosh, A. L., B. P. Atshaves, H. Huang, A. M. Gallegos, A. B. Kier, F. Schroeder, H. Xu, W. Zhang, and S. Liu. 2007. Multiphoton laser scanning microscopy and spatial analysis of dehydroergosterol distributions on plasma membranes of living cells. In *Lipid Rafts*. T. McIntosh, editor. Humana Press Inc., Totowa, NJ. 85–105.
- McIntosh, A. L., B. P. Atshaves, H. Huang, A. M. Gallegos, A. B. Kier, and F. Schroeder. 2008. Fluorescence techniques using dehydroergosterol to study cholesterol trafficking. *Lipids.* **43**: 1185–1208.
- McIntosh, A. L., H. Huang, B. P. Atshaves, S. M. Storey, A. Gallegos, T. A. Spencer, R. Bittman, Y. Ohno-Iwashita, A. B. Kier, and F. Schroeder. 2008. Fluorescent sterols for the study of cholesterol trafficking in living cells. In *Probes and Tags to Study Biomolecular Function for Proteins, RNA, and Membranes*. L. W. Miller, editor. Wiley VCH Verlag GmbH & Co., Weinheim. 1–33.
- Schroeder, F. 1984. Fluorescent sterols: probe molecules of membrane structure and function. (Review). *Prog. Lipid Res.* **23**: 97–113.
- Scheidt, H. A., P. Muller, A. Herrmann, and D. Huster. 2003. The potential of fluorescent and spin-labeled sterol analogues to mimic natural cholesterol. *J. Biol. Chem.* **278**: 45563–45569.
- Iwamoto, M., I. Morita, M. Fukuda, S. Murota, S. Ando, and Y. Ohno-Iwashita. 1997. A biotylated perfringolysin O derivative: a new probe for detection of cell surface cholesterol. *Biochim. Biophys. Acta.* **1327**: 222–230.
- Wiegand, V., T-Y. Chang, J. F. Strauss III, F. Fahrenholz, and G. Gimpl. 2003. Transport of plasma membrane derived cholesterol and the function of Niemann-Pick C1 protein. *FASEB J.* **17**: 782–784.
- Atshaves, B. P., S. M. Storey, and F. Schroeder. 2003. Sterol carrier protein-2/sterol carrier protein-x expression differentially alters fatty acid metabolism in L-cell fibroblasts. *J. Lipid Res.* **44**: 1751–1762.
- Atshaves, B. P., A. Gallegos, A. L. McIntosh, A. B. Kier, and F. Schroeder. 2003. Sterol carrier protein-2 selectively alters lipid composition and cholesterol dynamics of caveolae/lipid raft vs non-raft domains in L-cell fibroblast plasma membranes. *Biochemistry.* **42**: 14583–14598.
- Yancey, P. G., W. V. Rodrigueza, E. P. Kilsdonk, G. W. Stoudt, W. J. Johnson, M. C. Phillips, and G. H. Rothblat. 1996. Cellular cholesterol efflux mediated by cyclodextrins. *J. Biol. Chem.* **271**: 16026–16034.
- Christian, A. E., M. P. Haynes, M. C. Phillips, and G. H. Rothblat. 1997. Use of cyclodextrins for manipulating cellular cholesterol content. *J. Lipid Res.* **38**: 2264–2272.
- Atshaves, B. P., A. L. McIntosh, D. Landrock, H. R. Payne, J. Mackie, N. Maeda, J. M. Ball, F. Schroeder, and A. B. Kier. 2007. Effect of SCP-x gene ablation on branched-chain fatty acid metabolism. *Am. J. Physiol. Gastrointest. Liver Physiol.* **292**: 939–951.
- Gallegos, A. M., S. M. Storey, A. B. Kier, F. Schroeder, and J. M. Ball. 2006. Structure and cholesterol dynamics of caveolae/

- raft and nonraft plasma membrane domains. *Biochemistry* **45**: 12100–12116.
27. Storey, S. M., A. M. Gallegos, B. P. Atshaves, A. L. McIntosh, G. G. Martin, K. Landrock, A. B. Kier, J. A. Ball, and F. Schroeder. 2007. Selective cholesterol dynamics between lipoproteins and caveolae/lipid rafts. *Biochemistry* **46**: 13891–13906.
 28. Atshaves, B. P., J. R. Jefferson, A. L. McIntosh, B. M. McCann, K. Landrock, A. B. Kier, and F. Schroeder. 2007. Effect of sterol carrier protein-2 expression on sphingolipid distribution in plasma membrane lipid rafts/caveolae. *Lipids* **42**: 871–884.
 29. Frolov, A., A. Petrescu, B. P. Atshaves, P. T. C. So, E. Gratton, G. Serrero, and F. Schroeder. 2000. High density lipoprotein mediated cholesterol uptake and targeting to lipid droplets in intact L-cell fibroblasts. *J. Biol. Chem.* **275**: 12769–12780.
 30. Schroeder, F., Y. Barenholz, E. Gratton, and T. E. Thompson. 1987. A fluorescence study of dehydroergosterol in phosphatidylcholine bilayer vesicles. *Biochemistry* **26**: 2441–2448.
 31. Schroeder, F., G. Nemezc, Y. Barenholz, E. Gratton, and T. E. Thompson. 1988. Cholestatrienol time resolved fluorescence in phosphatidylcholine bilayers. *In Time Resolved Laser Spectroscopy in Biochemistry*. J. R. Lakowicz, M. Eftink, and J. Wampler, editors. SPIE Press, Bellingham. 457–465.
 32. Huang, H., J. A. Ball, J. T. Billheimer, and F. Schroeder. 1999. The sterol carrier protein-2 amino terminus: a membrane interaction domain. *Biochemistry* **38**: 13231–13243.
 33. Fischer, R. T., M. S. Cowlen, M. E. Dempsey, and F. Schroeder. 1985. Fluorescence of delta 5,7,9(11),22-ergostatetraen-3 beta-ol in micelles, sterol carrier protein complexes, and plasma membranes. *Biochemistry* **24**: 3322–3331.
 34. Schroeder, F., S. C. Myers-Payne, J. T. Billheimer, and W. G. Wood. 1995. Probing the ligand binding sites of fatty acid and sterol carrier proteins: effects of ethanol. *Biochemistry* **34**: 11919–11927.
 35. Willem, J., M. Beest, G. Scherphof, and D. Hoekstra. 1990. A non-exchangeable fluorescent phospholipid analogue as a membrane traffic marker of the endocytic pathway. *Eur. J. Cell Biol.* **53**: 173–184.
 36. Atshaves, B. P., O. Starodub, A. L. McIntosh, J. B. Roths, A. B. Kier, and F. Schroeder. 2000. Sterol carrier protein-2 alters HDL-mediated cholesterol efflux. *J. Biol. Chem.* **275**: 36852–36861.
 37. McIntosh, A. L., A. Gallegos, B. P. Atshaves, S. M. Storey, D. Kannoju, and F. Schroeder. 2003. Fluorescence and multiphoton imaging resolve unique structural forms of sterol in membranes of living cells. *J. Biol. Chem.* **278**: 6384–6403.
 38. Zhang, W., A. L. McIntosh, H. Xu, D. Wu, T. Gruninger, B. P. Atshaves, J. C. S. Liu, and F. Schroeder. 2005. Structural analysis of sterol distribution in the plasma membrane of living cells. *Biochemistry* **44**: 2864–2984.
 39. McIntyre, J. C., F. Schroeder, and W. D. Behnke. 1990. The interaction of bile salt micelles with the dansyltyrosine derivatives of porcine colipase. *Biophys. Chem.* **38**: 143–154.
 40. Bernik, D. L., and R. M. Negri. 1998. Local polarity at the polar head level of lipid vesicles using dansyl fluorescent probes. *J. Colloid. Interface Science.* **203**: 97–105.
 41. Haberland, M. E., and J. A. Reynolds. 1973. Self-association of cholesterol in aqueous solution. *Proc. Natl. Acad. Sci. USA.* **70**: 2313–2318.
 42. Avdulov, N. A., S. V. Chochina, U. Igbavboa, C. H. Warden, F. Schroeder, and W. G. Wood. 1999. Lipid binding to sterol carrier protein-2 is inhibited by ethanol. *Biochim. Biophys. Acta.* **1437**: 37–45.
 43. Mast, N., and I. A. Pikuleva. 2005. A simple and rapid method to measure cholesterol binding to P450s and other proteins. *J. Lipid Res.* **46**: 1561–1568.
 44. Spink, C. H., M. Yeager, and G. W. Feigenson. 1990. Partitioning behavior of indocarbocyanine probes between coexisting gel and fluid phases in model membranes. *Biochim. Biophys. Acta.* **1023**: 25–33.
 45. Schram, V., and T. E. Thompson. 1997. Influence of the intrinsic membrane protein bacteriorhodopsin on gel-phase domain topology in two-component phase-separated bilayers. *Biophys. J.* **72**: 2217–2225.
 46. Ohno-Iwashita, Y., Y. Shimada, A. A. Waheed, M. Hayashi, M. Inomata, M. Nakamura, M. Maruya, and S. Iwashita. 2004. Perfringolysin O, a cholesterol-binding cytolysin, as a probe for lipid rafts. *Anaerobe.* **10**: 125–134.
 47. Samsonov, A. V., I. Mihalyov, and F. S. Cohen. 2001. Characterization of cholesterol-sphingomyelin domains and their dynamics in bilayer membranes. *Biophys. J.* **81**: 1486–1500.
 48. de Almeida, R. F. M., L. M. S. Loura, A. Fedorov, and M. Prieto. 2005. Lipid rafts have different sizes depending on membrane composition: a time resolved fluorescence resonance energy transfer study. *J. Mol. Biol.* **346**: 1109–1120.
 49. Pike, L. J. 2003. Lipid rafts: bringing order to chaos. *J. Lipid Res.* **44**: 655–667.
 50. Lakowicz, J. R. 2006. Energy transfer. *In Principles of Fluorescence Spectroscopy*. J. R. Lakowicz, editor. Springer Science, New York, NY. 443–475.
 51. Dale, R. E., J. Eisinger, and W. E. Blumberg. 1979. The orientation freedom of molecular probes. *Biophys. J.* **26**: 161–193.
 52. Gallegos, A. M., A. L. McIntosh, B. P. Atshaves, and F. Schroeder. 2004. Structure and cholesterol domain dynamics of an enriched caveolae/raft isolate. *Biochem. J.* **382**: 451–461.
 53. Gallegos, A. M., B. P. Atshaves, A. L. McIntosh, S. M. Storey, J. M. Ball, A. B. Kier, and F. Schroeder. 2008. Membrane domain distributions: analysis of fluorescent sterol exchange kinetics. *Current Analytical Chemistry.* **4**: 1–7.
 54. Brown, D. A., and E. London. 1998. Structure and origin of ordered lipid domains in biological membranes. *J. Membr. Biol.* **164**: 103–114.
 55. Harroun, T. A., J. Katsaras, and S. R. Wassall. 2008. Cholesterol is found to reside in the center of a polyunsaturated lipid membrane. *Biochemistry* **47**: 7090–7096.
 56. Atshaves, B. P., A. L. McIntosh, H. R. Payne, A. M. Gallegos, K. Landrock, N. Maeda, A. B. Kier, and F. Schroeder. 2007. Sterol carrier protein-2/sterol carrier protein-x gene ablation alters lipid raft domains in primary cultured mouse hepatocytes. *J. Lipid Res.* **48**: 2193–2211.
 57. Pike, L. J., X. Han, K-N. Chung, and R. W. Gross. 2002. Lipid rafts are enriched in arachidonic acid and plasmenylethanolamine and their composition is independent of caveolin-1 expression: a quantitative electrospray ionization/mass spectrometric analysis. *Biochemistry* **41**: 2075–2088.
 58. Gallegos, A. M., B. P. Atshaves, S. M. Storey, A. L. McIntosh, A. D. Petrescu, and F. Schroeder. 2001. Sterol carrier protein-2 expression alters plasma membrane lipid distribution and cholesterol dynamics. *Biochemistry* **40**: 6493–6506.
 59. Schroeder, F., J. R. Jefferson, A. B. Kier, J. Knittell, T. J. Scallen, W. G. Wood, and I. Hapala. 1991. Membrane cholesterol dynamics: cholesterol domains and kinetic pools. *Proc. Soc. Exp. Biol. Med.* **196**: 235–252.
 60. Zhou, M., R. D. Parr, A. D. Petrescu, H. R. Payne, B. P. Atshaves, A. B. Kier, J. A. Ball, and F. Schroeder. 2004. Sterol carrier protein-2 directly interacts with caveolin-1 in vitro and in vivo. *Biochemistry* **43**: 7288–7306.
 61. Parr, R. D., G. G. Martin, H. A. Hostetler, M. E. Schroeder, K. D. Mir, A. B. Kier, J. M. Ball, and F. Schroeder. 2007. A new N-terminal recognition domain in caveolin-1 interacts with sterol carrier protein-2 (SCP-2). *Biochemistry* **46**: 8301–8314.
 62. Fielding, P. E., P. Chau, D. Liu, T. A. Spencer, and C. J. Fielding. 2004. Mechanism of platelet derived growth factor dependent caveolin-1 phosphorylation: relationship to sterol binding and the role of serine-80. *Biochemistry* **43**: 2578–2586.
 63. Chao, W. T., S-H. Tsai, Y-C. Lin, W-W. Lin, and V. C. Yang. 2005. Cellular localization and interaction of ABCA1 and caveolin-1 in aortic endothelial cells after HDL incubation. *Biochem. Biophys. Res. Commun.* **332**: 743–749.
 64. Assanases, C., C. Mineo, D. Seetharam, I. S. Yuhanna, Y. L. Marcel, M. A. Connelly, D. L. Williams, M. de la Llera-Moya, P. W. Shaul, and D. L. Silver. 2005. Cholesterol binding, efflux, and PDZ-interacting domain of scavenger receptor-B1 mediate HDL-initiated signaling. *J. Clin. Invest.* **115**: 969–977.
 65. Smart, E. J., Y. Ying, W. C. Donzell, and R. G. W. Anderson. 1996. A role for caveolin in transport of cholesterol from endoplasmic reticulum to plasma membrane. *J. Biol. Chem.* **271**: 29427–29435.
 66. Smart, E. J., and D. R. van der Westhuyzen. 1998. Scavenger receptors, caveolae, caveolin, and cholesterol trafficking. *In Intracellular Cholesterol Trafficking*. T. Y. Chang, and D. A. Freeman, editors. Kluwer Academic Publishers, Boston. 253–272.
 67. Pitto, M., J. Brunner, A. Ferraretto, D. Ravasi, P. Palestini, and M. Masserini. 2000. Use of a photoactivatable GM1 ganglioside analogue to assess lipid distribution in caveolae bilayer. *Glycoconj. J.* **17**: 215–222.

68. Schroeder, F. 1985. Fluorescence probes unravel asymmetric structure of membranes. (Review). *In* Subcellular Biochemistry. D. B. Roodyn, editor. Plenum Press, New York. 51–101.
69. Schroeder, F., G. Nemezc, W. G. Wood, C. Joiner, G. Morrot, M. Ayrault-Jarrier, and P. F. Devaux. 1991. Transmembrane distribution of sterol in the human eurythrocyte. *Biochim. Biophys. Acta.* **1066**: 183–192.
70. Everson, W. V., and E. J. Smart. 2001. Influence of caveolin, cholesterol, and lipoproteins on nitric oxide synthase. *Trends Cardiovasc. Med.* **11**: 246–250.